

1 **Simulation of ozone-vegetation coupling and feedback in**
2 **China using multiple ozone damage schemes**

3
4
5 Jiachen Cao¹, Xu Yue^{1*}, Mingrui Ma²
6

7 1. Jiangsu Key Laboratory of Atmospheric Environment Monitoring and Pollution
8 Control, Collaborative Innovation Center of Atmospheric Environment and Equipment
9 Technology, School of Environmental Science and Engineering, Nanjing University of
10 Information Science & Technology (NUIST), Nanjing, 210044, China

11 2. State Key Laboratory of Pollution Control and Resource Reuse, School of the
12 Environment, Nanjing University, Nanjing, 210044, China

13
14
15
16 *Corresponding author: Xu Yue

17 email: [yuexu@nuist.edu.cn](mailto:yuxu@nuist.edu.cn)
18
19
20
21
22
23
24

Abstract

As a phytotoxic pollutant, surface ozone (O_3) not only affects plant physiology but also influences meteorological fields and air quality by altering leaf stomatal functions. Previous studies revealed strong feedbacks of O_3 -vegetation coupling in China but with large uncertainties due to the applications of varied O_3 damage schemes and chemistry-vegetation models. In this study, we quantify the O_3 vegetation damage and the consequent feedbacks to surface meteorology and air quality in China by coupling two O_3 damage schemes (S2007 vs. L2013) into a fully coupled regional meteorology-chemistry model. With different schemes and damaging sensitivities, surface O_3 is predicted to decrease summertime gross primary productivity by 5.5%-21.4% and transpiration by 5.4%-23.2% in China, in which the L2013 scheme yields 2.5-4 times of losses relative to the S2007 scheme. The damages to photosynthesis of sunlit leaves are ~ 2.6 times that of shaded leaves in the S2007 scheme but show limited differences in the L2013 scheme. Though with large discrepancies in offline responses, the two schemes yield similar magnitude of feedback to surface meteorology and O_3 air quality. The O_3 -induced damage to transpiration increases national sensible heat by 3.2-6.0 W m^{-2} (8.9% to 16.2%) while reduces latent heat by 3.3-6.4 W m^{-2} (-5.6% to -17.4%), leading to a 0.2-0.51 $^{\circ}C$ increase in surface air temperature and a 2.2-3.9% reduction in relative humidity. Meanwhile, surface O_3 concentrations on average increase by 2.6-4.4 $\mu g m^{-3}$ due to the inhibitions of stomatal uptake and the anomalous enhancement in isoprene emissions, the latter of which is attributed to the surface warming by O_3 -vegetation coupling. Our results highlight the importance of O_3 control in China due to its adverse effects on ecosystem functions, global warming, and O_3 pollution through the O_3 -vegetation coupling.

Keywords: Ozone, vegetation, feedback, meteorology, air quality, regional model

52 **1 Introduction**

53 Surface ozone (O_3) is one of the most enduring air pollutants affecting air quality
54 in China, with detrimental effects on human health and ecosystem functions (Monk et
55 al., 2015). Long-term observations and numerical simulations have shown that O_3
56 affects stomatal conductance (Li et al., 2017), accelerates vegetation aging (Feng et al.,
57 2015), and reduces photosynthesis (Wittig et al., 2007). These negative effects altered
58 carbon allocation (Yue and Unger, 2014; Lombardozzi et al., 2015) and inhibited plant
59 growth (Li et al., 2016), suppressing ecosystem carbon uptake (Ainsworth, 2012).
60 Moreover, these effects have profound implications for global/regional climate and
61 atmospheric environment. Given the significant ecological impacts, a systematic
62 quantification of the O_3 vegetation damage effect in China is of great importance for
63 the better understanding of the side effects of O_3 pollution on both regional carbon
64 uptake and climate change.

65 At present, field experiments on O_3 -induced vegetation damage have been
66 conducted in China but were mostly confined to individual monitoring sites. For
67 instance, Su et al. (2017) conducted experiments on grassland in Inner Mongolia and
68 found that elevated O_3 concentrations resulted in a decrease of approximately 20% in
69 the photosynthetic rate of herbaceous plants. Meta-analysis of tropical, subtropical, and
70 temperate tree species in China found that increased O_3 concentrations reduced net
71 photosynthesis and total biomass of Chinese woody plants by 28% and 14%,
72 respectively (Li et al., 2017). However, most of these experiments were conducted
73 using open-top chambers with artificially controlled O_3 concentrations, rather than
74 actual surface O_3 concentrations, making it difficult to quantitatively estimate the
75 impact of ambient O_3 on vegetation productivity. Furthermore, the spatial coverage of
76 field experiments is limited, which hinders the direct use of observational data for
77 assessing O_3 vegetation damage in different regions of China.

78 Alternatively, numerical models provide a more feasible approach to quantify the
79 O_3 -induced vegetation damage from the regional to global scales. Currently, there are
80 three main parameterizations for the calculation of ozone vegetation damage. Felzer et

81 al. (2004) established an empirical scheme based on the Accumulated Ozone exposure
82 over a Threshold of 40 ppb (AOT40) within the framework of a terrestrial ecosystem
83 model. They further estimated that O₃ pollution in the United States led to a decrease
84 in net primary productivity (NPP) by 2.6% to 6.8% during the period of 1980-1990.
85 However, the AOT40 is related to O₃ concentrations alone and ignores the biological
86 regulations on the O₃ stomatal uptake, leading to inconsistent tendencies between O₃
87 pollution level and plant damage at the drought conditions (Gong et al., 2021). In
88 acknowledge of such deficit, Sitch et al. (2007) proposed a semi-mechanistic scheme
89 calculating O₃ vegetation damage based on the stomatal uptake of O₃ fluxes and the
90 coupling between stomatal conductance and leaf photosynthesis. Yue and Unger (2014)
91 implemented this scheme into the Yale Interactive terrestrial Biosphere (YIBs) model.
92 Taking into account varied O₃ sensitivities of different vegetation types, they estimated
93 that surface O₃ led to reductions of 2-5% in the summer gross primary productivity
94 (GPP) in eastern U.S. from 1998 to 2007. Later, Lombardozzi et al. (2013) conducted
95 a meta-analysis using published chamber data and found different levels of responses
96 to O₃ exposure between stomatal conductance and photosynthesis. They further
97 implemented the independent response relationships into the Community Land Model
98 (CLM) and estimated that current ozone levels led to a reduction in global GPP by 8%-
99 12% (Lombardozzi et al., 2015).

100 The O₃ stress on vegetation physiology can feed back to affect regional climate.
101 Lombardozzi et al. (2015) employed the CLM model and found that current O₃
102 exposure reduced transpiration by 2%-2.4% globally and up to 15% regionally over
103 eastern U.S., Europe, and Southeast Asia, leading to further perturbations in surface
104 energy balance. In U.S., Li et al. (2016) found that the O₃ vegetation damage reduced
105 latent heat (LH) flux, precipitation, and runoff by 10-27 W m⁻², 0.9-1.4 mm d⁻¹, and
106 0.1-0.17 mm d⁻¹, respectively, and increased surface air temperature by 0.6-2.0 °C
107 during the summer of 2007-2012. In China, Zhu et al. (2022) performed simulations
108 and found that the inclusion of O₃-vegetation interaction caused a 5-30 W m⁻² decrease
109 in LH, 0.2-0.8 °C increase in surface air temperature, and 3% reduction in relative

110 humidity during summers of 2014-2017. Recently, Jin et al. (2023) applied a different
111 regional model and estimated that O₃ exposure weakened plant transpiration and altered
112 surface heat flux in China, resulting in significant increase of up to 0.16 °C in maximum
113 daytime temperature and decrease of -0.74% in relative humidity. However, all these
114 previous estimates of O₃-induced feedback to climate were derived using the empirical
115 O₃ damage scheme proposed by Lombardozzi et al. (2013), which assumed fixed
116 damage ratios independent of O₃ dose for some vegetation species and as a result may
117 have biases in the further estimated feedback to climate.

118 The O₃-vegetation coupling also has intricate implications for air quality. On one
119 hand, O₃-vegetation coupling can influence meteorological conditions that affect O₃
120 generation, ultimately influencing the O₃ level (Sadiq et al., 2017). On the other hand,
121 it can also influence biogenic emissions and dry deposition, thereby affecting O₃
122 concentrations (Gong et al., 2020). Sadiq et al. (2017) implemented O₃-vegetation
123 coupling in the Community Earth System Model (CESM) and estimated that surface
124 O₃ concentrations increased 4-6 ppb in Europe, North America, and China due to O₃-
125 vegetation coupling. By using the CLM model with the empirical scheme of
126 Lombardozzi et al. (2013), Zhou et al. (2018) found that O₃-induced damage on leaf
127 area index (LAI) could lead to changes in global O₃ concentrations by -1.8 to +3 ppb
128 in boreal summer. Gong et al., (2020) used the O₃ damage scheme from Sitch et al.
129 (2007) embedded in a global climate-chemistry-carbon coupled model and estimated
130 that O₃-induced stomatal inhibition led to an average surface O₃ increase of 1.2-2.1 ppb
131 in eastern China and 1.0-1.3 ppb in western Europe. Different from the above global
132 simulations with coarse resolutions, regional modeling with fine resolution can reveal
133 more details about O₃-vegetation coupling and feedback to surface O₃ concentrations
134 in China (Zhu et al., 2022; Jin et al., 2023). However, all these regional simulations
135 were carried out using O₃ damage scheme of Lombardozzi et al. (2013), limiting the
136 exploration of model uncertainties due to varied O₃ vegetation damage schemes.

137 In this study, we implemented O₃ vegetation damage schemes from both Sitch et
138 al. (2007) and Lombardozzi et al. (2013) into the widely-used regional meteorology-

139 chemistry model WRF-Chem. We validated the simulated meteorology and O₃
140 concentrations, and performed sensitivity experiments to explore the O₃ damage to GPP
141 and consequent feedbacks to regional climate and air quality in China. Within the same
142 framework, we compared the differences of O₃-vegetation coupling from two schemes
143 and explored the causes for the discrepancies. We aimed to quantify the modeling
144 uncertainties in the up-to-date estimates of O₃ impact on regional carbon fluxes and its
145 feedback to regional climate and air quality in China.

146

147 **2 Method**

148 **2.1 WRF-Chem model**

149 We used WRF-Chem model version 3.9.1 to simulate meteorological fields and
150 O₃ concentration in China. The model includes atmospheric physics and dynamical
151 processes, atmospheric chemistry, and biophysical and biochemical processes (Grell et
152 al., 2005, Skamarock et al., 2008). The model domain is configured with 196×160 grid
153 cells at 27 km horizontal resolution on the Lambert conformal projection, and covers
154 the entire mainland China. In the vertical direction, 28 layers are set extending from
155 surface to 50 hPa. The meteorological initial and boundary conditions were adopted
156 from ERA5 reanalysis produced by the European Centre for Medium-Range Weather
157 Forecasts (ECMWF) at a horizontal resolution of 0.25°×0.25° (Hersbach et al., 2020).
158 The chemical initial and boundary conditions were generated from the Model for Ozone
159 and Related Chemical Tracer version 4 (MOZART-4), which is available at a horizontal
160 resolution of 1.9°×2.5° with 56 vertical layers (Emmons et al., 2010).

161 Anthropogenic emissions are adopted from the 0.25° Multi-resolution Emission
162 Inventory for China (MEIC) and MIX Asian emission inventory for the other regions
163 (available at <http://meicmodel.org>). Biogenic emissions are calculated online using the
164 Model of Emissions of Gases and Aerosols from Nature (Guenther et al., 2006), which
165 considers the impacts of plant types, weather conditions, and leaf area on vegetation
166 emissions. Atmospheric chemistry is simulated using the Carbon Bond Mechanism
167 version Z (CBMZ) (Zaveri and Peters, 1999) gas-phase chemistry module coupled with

168 a four-bin sectional Model for Simulating Aerosol Interactions and Chemistry
 169 (MOSAIC) (Zaveri et al., 2008). The photolysis scheme is based on the Madronich
 170 Fast-TUV photolysis module (Tie et al., 2003). The physical configurations include the
 171 Morrison double-moment microphysics scheme (Morrison et al., 2009), the Grell-3
 172 cumulus scheme (Grell et al., 2002), the Rapid Radiative Transfer Model longwave
 173 radiation scheme (Mlawer et al., 1997), the Goddard short-wave radiation scheme
 174 (Chou and Suarez, 1994), the Yonsei University planetary boundary layer scheme
 175 (Hong et al., 2006), and the revised MM5 (Fifth generation Mesoscale Model) Monin–
 176 Obukhov surface layer scheme.

177

178 **2.2 Noah-MP model**

179 Noah-MP is a land surface model coupled to WRF-Chem with multiple options
 180 for key land-atmosphere interaction processes (Niu et al., 2011). Noah-MP considers
 181 canopy structure with canopy height and crown radius, and depicts leaves with
 182 prescribed dimensions, orientation, density, and radiometric properties. The model
 183 employs a two-stream radiative transfer approach for surface energy and water transfer
 184 processes (Dickinson, 1983). Noah-MP is capable of distinguishing photosynthesis
 185 pathways between C₃ and C₄ plants, and defines vegetation-specific parameters for leaf
 186 photosynthesis and respiration.

187 Noah-MP considers prognostic vegetation growth through the coupling between
 188 photosynthesis and stomatal conductance (Farquhar et al., 1980; Ball et al., 1987). The
 189 photosynthesis rate, A ($\mu\text{molCO}_2 \text{ m}^{-2} \text{ s}^{-1}$), is calculated as one of three limiting factors
 190 as follows:

$$191 \quad A_{tot} = \min(W_c, W_j, W_e)I_{gs} \quad (1)$$

192 where W_c is the RuBisco-limited photosynthesis rate, W_j is the light-limited
 193 photosynthesis rate, and W_e is the export-limited photosynthesis rate. I_{gs} is the
 194 growing season index with values ranging from 0 to 1. Stomatal conductance (g_s) is
 195 computed based on photosynthetic rate as follows:

$$196 \quad g_s = \frac{1}{r_s} = m \frac{A_{net}}{C_s} RH + b \quad (2)$$

197 where b is the minimum stomatal conductance; m is the Ball-Berry slope of the
 198 conductance-photosynthesis relationship; A_{net} is the net photosynthesis by subtracting
 199 dark respiration from A_{tot} ; C_s is the ambient CO₂ concentration at the leaf surface. The
 200 assimilated carbon is allocated to various parts of vegetation (leaf, stem, wood, and root)
 201 and soil carbon pools (fast and slow), which determines the variations of LAI and
 202 canopy height. Plant transpiration rate is then estimated using the dynamic LAI and
 203 stomatal conductance. Noah-MP also distinguishes the photosynthesis of sunlit and
 204 shaded leaves. Sunlit leaves are more limited by CO₂ concentration while shaded leaves
 205 are more constrained by insolation, leading to varied responses to O₃ damage.

206

207 **2.3 Scheme for ozone damage on vegetation**

208 We implemented the O₃ vegetation damage schemes proposed by Sitch et al. (2007)
 209 (thereafter S2007) and Lombardozzi et al. (2013) (thereafter L2013) into the Noah-MP.
 210 In S2007 scheme, the undamaged fraction F for net photosynthesis is dependent on the
 211 sensitivity parameter a_{PFT} and excessive area-based stomatal O₃ flux, which is
 212 calculated as the difference between f_{O_3} and threshold y_{PFT} :

$$213 \quad F = 1 - a_{PFT} \times \max\{f_{O_3} - y_{PFT}, 0\} \quad (3)$$

214 where a_{PFT} and y_{PFT} are specifically determined for individual plant functional types
 215 (PFTs) based on measurements (Table 1). The stomatal O₃ flux f_{O_3} is calculated as

$$216 \quad f_{O_3} = \frac{[O_3]}{r_a + k_{O_3} \cdot r_s} \quad (4)$$

217 where $[O_3]$ is the O₃ concentration at the reference level (nmol m⁻³), r_a is the
 218 aerodynamic and boundary layer resistance between leaf surface and reference level (s
 219 m⁻¹). $k_{O_3} = 1.67$ represents the ratio of leaf resistance for O₃ to that for water vapor. r_s
 220 represents stomatal resistance (s m⁻¹). For S2007 scheme, stomatal conductance is
 221 damaged with the same ratio (1- F) as photosynthesis and further affects O₃ uptake. In
 222 Noah-MP, the f_{O_3} are calculated separately for sunlit and shaded leaves with
 223 corresponding stomatal resistance (Supplementary Text S1).

224 As a comparison, the L2013 scheme applies separate O₃ damaging relationships

225 for photosynthetic rate and stomatal conductance. These independent relationships
226 account for different plant groups and are calculated based on the cumulative uptake of
227 O₃ (CUO) under different levels of chronic O₃ exposure. The leaf-level CUO (mmol m⁻²)
228 over the growing season is calculated as follows:

$$229 \quad CUO = \sum(k_{O_3}/r_s + 1/r_a) \times [O_3] \quad (5)$$

230 The physical parameters in Equation (5) are the same as those in Equation (4). O₃ uptake
231 is accumulated over time steps during the growing season with mean LAI > 0.5
232 (Lombardozzi et al., 2012), when vegetation is most vulnerable to air pollution episodes.
233 O₃ uptake is only accumulated when O₃ flux is above an instantaneous threshold of 0.8
234 nmol O₃ m⁻² s⁻¹ to account for ozone detoxification by vegetation at low O₃ levels
235 (Lombardozzi et al., 2015). We also include a leaf-turnover rate for evergreen plants so
236 that the accumulation of O₃ flux does not last beyond the average foliar lifetime. The
237 O₃ damaging ratios depend on CUO with empirical linear relationships as follows:

$$238 \quad F_{pO_3} = a_p \times CUO + b_p \quad (6)$$

$$239 \quad F_{cO_3} = a_c \times CUO + b_c \quad (7)$$

240 where F_{pO_3} and F_{cO_3} are the ozone damage ratios for photosynthesis and stomatal
241 conductance, respectively. The slopes (a_p for photosynthesis and a_c for stomatal
242 conductance) and intercepts (b_p for photosynthesis and b_c for stomatal conductance) of
243 regression functions are determined based on the meta-analysis of hundreds of
244 measurements (Table 2). The ratios predicted in Equations (6) and (7) are applied to
245 photosynthesis and stomatal conductance, respectively, to account for their independent
246 responses to O₃ damages. In Noah-MP, the F_{pO_3} and F_{cO_3} are calculated separately for
247 sunlit and shaded leaves based on corresponding stomatal resistance (Supplementary
248 Text S1).

249

250 **2.4 Observational data**

251 We validated the simulated meteorology and air pollutants with observations. The
252 meteorological data were downloaded from the National Meteorological Information
253 Center of China Meteorological Administration (CMA Meteorological Data Centre,

254 2022, <http://data.cma.cn/data/detail/dataCode/A.0012.0001.html>). The daily averaged
255 surface pressure (PRES), wind speed at a height of 10 m (WS10), relative humidity
256 (RH) and temperature at a height of 2 m (T2) were collected from 839 ground stations.
257 Hourly surface O₃ concentrations at 1597 sites in China were collected from Chinese
258 National Environmental Monitoring Center (CNEMC, <http://websearch.mep.gov.cn/>).

259

260 **2.5. Simulations**

261 We performed seven experiments to quantify the damaging effects of ambient O₃
262 on GPP and the feedbacks to regional climate and air quality (Table 3). All simulations
263 are conducted from 1st May to 31st August of 2017 with the first month excluded from
264 the analysis as the spin-up. The control simulations (CTRL) excluded the impact of
265 ozone on vegetation. Three offline simulations were performed with the same settings
266 as the CTRL run, except that O₃ vegetation damages were calculated and output without
267 feedback to affect vegetation growth. These offline runs were established using either
268 the S2007 scheme (Offline_SH07 for high sensitivity and Offline_SL07 for low
269 sensitivity) or the L2013 scheme (Offline_L13). As a comparison, three online
270 simulations applied the S2007 scheme (Online_SH07 for high sensitivity and
271 Online_SL07 for low sensitivity) and the L2013 scheme (Online_L13) to estimate the
272 O₃ damages to GPP, which further influenced LAI development, leaf transpiration, and
273 dry deposition. The differences between CTRL and Online runs indicated the responses
274 of surface meteorology and O₃ concentrations to the O₃-induced vegetation damages.

275

276 **3. Results**

277 **3.1 Model evaluations**

278 We compared the simulated summer near-surface temperature, relative humidity,
279 wind speed, and surface O₃ concentrations to observations. The model reasonably
280 reproduces the spatial pattern of higher near-surface temperature in Southeast and
281 Northwest and lower temperature over the Tibetan Plateau (Figure 1a). On the national
282 scale, the near-surface temperature is underestimated with a mean bias (MB) of 1.04 °C

283 but it shows a high correlation ($R=0.96$). Unlike temperature, simulated relative
284 humidity is overestimated with a MB of 5.04 % but a high R of 0.93 (Figure 1b). Due
285 to the modeling biases in the topographic effects, simulated wind speed is overestimated
286 by more than 1.06 m s^{-1} on the national scale (Figure 1c). Such overestimation was also
287 reported in other studies using WRF models (Hu et al., 2016, Liu et al., 2020, Zhu et
288 al., 2022).

289 Comparisons with the measurements from air quality sites show that the simulated
290 O_3 deviates from the observed mean concentrations by $5.42 \mu\text{g m}^{-3}$ with a spatial R of
291 0.68. The model reasonably captures the hotspots over North China Plain though with
292 some overestimations, potentially attributed to uncertain emissions and coarse model
293 resolutions. Such elevated bias in summer O_3 is a common issue for both global and
294 regional models over Asia. For example, Zhu et al. (2022) reported the overestimated
295 summer average ozone concentration by $13.82 \mu\text{g m}^{-3}$ in China. Liu et al. (2020)
296 reached positive biases ranging from $3.7 \mu\text{g m}^{-3}$ to $13.32 \mu\text{g m}^{-3}$ using the WRF-CMAQ
297 model. Overall, the WRF-Chem model shows reasonable performance in the simulation
298 of surface meteorology and O_3 concentrations in China.

299

300 **3.2 Offline O_3 damage**

301 We compared the offline O_3 damage to photosynthesis between sunlit (PSNSUN)
302 and shaded (PSNSHA) leaves during the summer. The S2007 scheme is dependent on
303 instantaneous O_3 uptake, which peaks when both O_3 concentrations and stomatal
304 conductance are high. For the same O_3 pollution level, the damages are much higher
305 for the sunlit leaves (Figures 2a-2b) than that for the shaded leaves (Figures 2d-2e),
306 because of the higher stomatal conductance linked with the more active photosynthesis
307 for the sunlit leaves. In contrast, the L2013 scheme depends on the accumulated O_3 flux
308 and assumes constant damages for some PFTs (Table 2), resulting in reductions of
309 photosynthesis even at low O_3 concentrations. Consequently, we found limited
310 differences in the O_3 damages between sunlit (Figure 2c) and shaded (Figure 2f) leaves
311 with L2013 scheme. Observations have reported that surface O_3 has limited impacts on

312 the shaded leaves (Wan et al., 2014), consistent with the results simulated by the S2007
313 scheme.

314 Figure 3 shows the effect of O₃ damage to stomatal resistance of sunlit (RSSUN)
315 and shaded (RSSHA) leaves. Overall, the spatial pattern of the changes in stomatal
316 resistance is consistent with those of photosynthesis (Figure 2) but with opposite signs.
317 Both RSSUN and RSSHA are enhanced by O₃ damage so as to prevent more O₃ uptake.
318 For S2007 scheme, RSSUN with high and low sensitivities respectively increases by
319 13.43% (Figure 3a) and 8.35% (Figure 3b), higher than the rates of 4.71% (Figure 3d)
320 and 2.97% (Figure 3e) for RSSHA. These ratios are inversely connected to the changes
321 of photosynthesis (Figure 2), suggesting the full coupling of damages between leaf
322 photosynthesis and stomatal conductance. For L2013 scheme, predicted changes in
323 RSSUN (Figure 3c) and RSSHA (Figure 3f) are very similar with the magnitude of
324 25.3%-26.3%. These changes are higher than the loss of photosynthesis (Figures 2c and
325 2f), suggesting the decoupling of O₃ damages to leaf photosynthesis and stomatal
326 conductance as revealed by the L2013 scheme.

327 We further assessed the O₃ damage to GPP and transpiration (TR). For S2007
328 scheme, O₃ causes damages to national average GPP and TR approximately by 5.5%
329 with low sensitivity (Figures 4b and 4e) and 8.4% with high sensitivity (Figures 4a and
330 4d) compared to the CTRL simulation. The model predicts high GPP damages over
331 North China Plain and moderate damages in the southeastern and northeastern regions.
332 In the northwest, GPP damage is very limited due to the low relative humidity (Figure
333 1b) that constrains the stomatal uptake. For L2013 scheme, TR shows uniform
334 reductions exceeding -25% in most regions of China except for the northwest (Figure
335 4f), though O₃ concentrations show distinct spatial gradient (Figure 1d). The changes
336 of GPP are similar to that of TR but with lower inhibitions (Figure 4c). On average, the
337 GPP reduction with the L2013 scheme is 2.5-3.9 times of that predicted with the S2007
338 scheme. The most significant differences are located in Tibetan Plateau with limited
339 damages in S2007 but strong inhibitions of both GPP and TR in L2013. The low
340 temperature (Figure 1a) and O₃ concentrations (Figure 1d) jointly constrain O₃ stomatal

341 uptake (Figure S2), leading to low O₃ damages over Tibetan Plateau with the S2007
342 scheme. However, the L2013 scheme applies $b_p=0.8021$ for grassland (Table 2),
343 suggesting strong baseline damages up to 20% even with CUO=0 over Tibetan Plateau
344 where the grassland dominates (Figure S3).

345

346 **3.3 The O₃-vegetation feedback to surface energy and meteorology**

347 The O₃ vegetation damage causes contrasting responses in surface sensible heat
348 (SH) and LH (Figure 5). For S2007 scheme, the SH fluxes on average increase by 3.17
349 W m⁻² (8.85%) with low sensitivity (Figure 5b) and 5.99 W m⁻² (16.22%) with high
350 sensitivity (Figure 5a). The maximum enhancement is located in southern China, where
351 the increased stomatal resistance (Figure 3a) reduces transpiration and the consequent
352 heat dissipation. Meanwhile, LH fluxes decrease by 3.26 W m⁻² (5.58%) with low
353 sensitivity (Figure 5e) and 6.43 W m⁻² (15.29%) with high sensitivity (Figure 5d),
354 following the reductions in transpiration (Figures 4d and 4e). We found similar changes
355 in surface energy by O₃-vegetation coupling between the S2007 and L2013 schemes.
356 The SH shows the same hotspots over southern China with national average increase
357 of 12.85% (Figure 5c), which is within the range of 8.85% to 16.22% predicted by the
358 S2007 scheme. The LH largely decreases in central and northern China with the mean
359 reduction of 17.4% (Figure 5f), close to the magnitude of 15.29% predicted with the
360 S2007 scheme using the high O₃ sensitivity (Figure 5d). Although the offline damages
361 to GPP and TR are much larger with the L2013 than S2007 (Figure 4), their feedback
362 to surface energy shows consistent spatial pattern and magnitude (Figure 5), likely
363 because the O₃ inhibition in S2007 has the same diurnal cycle with energy fluxes while
364 the L2013 scheme shows almost constant inhibitions throughout the day (Figure S1).
365 The zero or near-zero slope parameters (a_p and a_c) in the L2013 scheme (Table 2) lead
366 to insensitive responses of photosynthesis and stomatal conductance to the variations
367 of CUO. As a result, there were very limited diurnal variations in O₃ damage with the
368 L2013 scheme. However, the strong nighttime damages in L2013 have limited
369 contributions to the changes of surface energy, which usually peaks at the daytime.

370 The O₃-induced damages to stomatal conductance weaken plant transpiration and
371 thus slow down the heat dissipation at the surface, leading to the higher temperature but
372 lower RH in China (Figure 6). On the national scale, temperature increases by 0.5 °C
373 due to O₃ vegetation damage with the high sensitivity (Figure 6a) and 0.23 °C with the
374 low sensitivity (Figure 6b) predicted using the S2007 scheme. A similar warming is
375 predicted with the L2013 scheme except that temperature shows moderate enhancement
376 over Tibetan Plateau (Figure 6c). The average RH decreases by 3.68% with the high O₃
377 sensitivity (Figure 6d) and 2.22% with the low sensitivity (Figure 6e) in response to the
378 suppressed plant transpiration. A stronger RH reduction of -3.85% is achieved with the
379 L2013 scheme, which predicts the maximum RH reductions in the North (Figure 6f).

380

381 **3.4 The O₃-vegetation feedback to air quality**

382 The O₃-induced inhibition on stomatal resistance leads to a significant increase in
383 surface O₃ concentrations, particularly in eastern China (Figures 7a-7c). The main cause
384 of such feedback is the reduction in O₃ dry deposition, which exacerbates the O₃
385 pollution in China. For S2007 scheme, this positive feedback can reach up to 15 µg m⁻³
386 with high sensitivity (Figure 7a) and 8 µg m⁻³ with low sensitivity (Figure 7b) over
387 North China Plain. On the national scale, surface O₃ enhances 4.40 µg m⁻³ (5.08 %)
388 with high O₃ sensitivity and 2.62 µg m⁻³ (3.04%) with low O₃ sensitivity through the
389 coupling to vegetation. For L2013 scheme, the changes of O₃ concentration (Figure 7c)
390 are comparable to that of the S2007 scheme with high sensitivity (Figure 7a), except
391 that the O₃ enhancement is stronger in the Southeast but weaker in the Northeast.

392 The O₃-vegetation coupling also increases surface isoprene emissions. For S2007
393 scheme, isoprene emissions increase by 6.13% with high sensitivity (Figure 7d) and
394 3.43% with low sensitivity (Figure 7e), with regional hotspots in North China Plain,
395 northeastern and southern regions. The predictions using L2013 scheme (Figure 7f)
396 show very similar patterns and magnitude of isoprene changes to the S2007 scheme
397 with high sensitivity. Such enhancement in isoprene emissions is related to the
398 additional surface warming by O₃-vegetation interactions (Figures 6a-6c). In turn, the

399 increased isoprene emissions contribute to the deterioration of O₃ pollution in China.

400

401 **4. Conclusions and discussion**

402 In this study, we explored the feedback of O₃-vegetation coupling to surface
403 meteorology and air quality in China using two O₃ damage schemes embedded in a
404 regional meteorology-chemistry coupled model. The two schemes predicted distinct
405 spatial patterns with much larger magnitude of GPP loss in the L2013 scheme than that
406 in the S2007 scheme. We further distinguished the leaf responses with different
407 illuminations. For the S2007 scheme, the damages to photosynthesis of sunlit leaves
408 are ~2.6 times of that to shaded leaves. However, for the L2013 scheme, limited
409 differences are found between the sunlit and shaded leaves. The damages to leaf
410 photosynthesis increase stomatal resistance, leading to the reductions of transpiration
411 but enhancement of sensible heat due to the less efficient heat dissipation. These
412 changes in surface energy and water fluxes feed back to increase surface temperature
413 but decrease relative humidity. Although the L2013 scheme predicts much stronger
414 offline damages, the feedback causes very similar pattern and magnitude in surface
415 warming as the S2007 scheme. Consequently, surface O₃ increases due to the stomatal
416 closure and isoprene emissions enhance due to the anomalous warming.

417 Our predicted O₃ damage to GPP was within the range of -4% to -40% as estimated
418 in previous studies using different models and/or parameterizations over China (Ren et
419 al., 2011; Lombardozzi et al., 2015; Yue et al., 2015; Sadiq et al., 2017; Xie et al., 2019;
420 Zhu et al., 2022; Jin et al., 2023). Such a wide span revealed the large uncertainties in
421 the estimate of O₃ impacts on ecosystem functions. In this study, we employed two
422 schemes and compared their differences. With the S2007 scheme, we predicted GPP
423 reductions of -5.5% to -8.5% in China. This is similar to the range of -4% to -10%
424 estimated by Yue et al. (2015) using the same O₃ damage scheme. However, it is lower
425 than the estimate of -12.1% predicted by Xie et al. (2019), likely due to the slight
426 overestimation of surface O₃ in the latter study. With the L2013 scheme, we predicted
427 much larger GPP reductions of -21.4%. However, such value was still lower than the -

428 28.9% in Jin et al. (2023) and -20% to -40% in Zhu et al. (2022) using the same L2013
429 scheme embedded in WRF-Chem model, though all studies showed similar spatial
430 patterns in the GPP reductions. Such differences were likely attributed to the varied
431 model configuration as we ran the model from May while the other studies started from
432 the beginning of years. The longer time for the accumulation of O₃ stomatal uptake in
433 other studies might result in higher damages than our estimates with the L2013 scheme.

434 The O₃-vegetation coupling caused strong feedback to surface meteorology and
435 air quality. Our simulations with either scheme revealed that surface SH increases by
436 2-28 W m⁻² and LH decreases by 4-32 W m⁻² over eastern China, consistent with the
437 estimates of 5-30 W m⁻² by Zhu et al. (2022) using WRF-Chem model with the L2013
438 scheme. Consequently, surface air temperature on average increases by 0.23-0.51°C
439 while relative humidity decreases by 2.2-3.8%, similar to the warming of 0.2-0.8°C and
440 RH reduction of 3% as predicted by Zhu et al. (2022). However, these changes in
441 surface energy flux and meteorology are much higher than that in Jin et al. (2023),
442 likely because the latter focuses on the perturbations averaged throughout the year
443 instead of summer period as in this study and Zhu et al. (2022). We further predicted
444 that O₃ vegetation damage increased surface O₃ by 1.0-3.33 μg m⁻³ in China, similar
445 to the 2.35-4.11 μg m⁻³ estimated for eastern China using a global model (Gong et al.,
446 2020). Regionally, the O₃ enhancement reached as high as 7.84-14.70 μg m⁻³ in North
447 China Plain, consistent with the maximum value of 11.76 μg m⁻³ over the same domain
448 predicted by Zhu et al. (2022). However, limited feedback to surface O₃ was predicted
449 in Jin et al. (2023), mainly because the decreased dry deposition had comparable but
450 opposite effects to the decreased isoprene emissions due to the reductions of LAI. Such
451 discrepancy was likely caused by the stronger O₃ inhibition in Jin et al. (2023) following
452 the longer period of O₃ accumulation, consequently exacerbating the negative impacts
453 of LAI reductions on O₃ production.

454 There were some limitations in our parameterizations and simulations. First, we
455 predicted increases of isoprene emissions in eastern China mainly due to the increased
456 leaf temperature, which is in line with previous studies (Sadiq et al., 2017; Zhu et al.,

457 2022). However, isoprene production is coupled to photosynthesis. There are empirical
458 evidences showing that high dose of O₃ exposure reduces isoprene emissions when O₃
459 exposure is prolonged enough to suppress photosynthesis (Bellucci et al., 2023).
460 Inclusion of such negative feedback might alleviate the O₃-induced enhancement in
461 isoprene emissions. Second, the WRF-Chem model slightly overestimated summer O₃
462 concentrations, which could exacerbate the damages to stomatal conductance and the
463 subsequent feedback. Third, the S2007 scheme employed the coupled responses in
464 photosynthesis and stomatal conductance to O₃ vegetation damage. However, some
465 observations revealed that stomatal response is slow under long-term O₃ exposure,
466 resulting in loss of stomatal function and decoupling from photosynthesis (Calatayud
467 et al., 2007; Lombardozzi et al., 2012). The L2013 scheme considered the decoupling
468 between photosynthesis and stomatal conductance. However, this scheme shows no
469 significant different changes for sunlit and shaded leaves. In addition, the calculation
470 of CUO heavily relied on the O₃ threshold and accumulation period, leading to varied
471 responses among different studies using the same scheme. Furthermore, the slopes of
472 O₃ sensitivity in L2013 scheme were set to zero for some PFTs, leading to constant
473 damages independent of CUO. Fourth, the current knowledge of the O₃ effects on
474 stomatal conductance was primarily derived from leaf-level measurements (Matyssek
475 et al., 2008), which were much fewer compared to that for photosynthesis. The limited
476 data availability and lack of inter-PFT responses constrain the development of empirical
477 parameterizations.

478 Despite these limitations, our study provided the first comparison of different
479 parameterizations in simulating O₃-vegetation interactions. We found similar feedbacks
480 to surface energy and meteorology though the two schemes showed varied magnitude
481 and distribution in the offline responses of GPP and stomatal conductance to surface
482 O₃. The main cause of such inconsistency lied in the low feedback of damages in L2013
483 with some unrealistic inhibitions of ecosystem functions at night and over the regions
484 with low O₃ level. Such similarity provides a solid foundation for the exploration of
485 O₃-vegetation coupling using different schemes. The positive feedback of O₃ vegetation

486 damage to surface air temperature and O₃ concentrations posed emerging but ignored
487 threats to both climate change and air quality in China.

488

489 **Data availability.** The observed hourly O₃ concentrations were obtained from Chinese
490 National Environmental Monitoring Center (CNEMC, <http://websearch.mep.gov.cn/>).
491 The observed meteorological data were obtained from the National Meteorological
492 Information Center of China Meteorological Administration (CMA Meteorological
493 Data Centre, 2022, <http://data.cma.cn/data/detail/dataCode/A.0012.0001.html>). The
494 MEIC and MIX emission inventory are available at
495 http://meicmodel.org.cn/?page_id=560 and http://meicmodel.org.cn/?page_id=89.

496

497 **Author contributions.** XY conceived the study. XY and JC designed the research and
498 carried out the simulations. JC completed data analysis and the first draft. MM provided
499 useful comments on the paper. XY reviewed and edited the manuscript.

500

501 **Competing interests.** The authors declare that they have no conflict of interest.

502

503 **Acknowledgements.** The authors are grateful to three anonymous reviewers for their
504 constructive comments that have improved this study.

505

506 **Financial support.** This study was jointly funded by the National Key Research and
507 Development Program of China (grant no. 2023YFF0805403), National Natural
508 Science Foundation of China (grant no. 42293323), and Jiangsu Funding Program for
509 Excellent Postdoctoral Talent (grant no. 2023ZB737).

510

511 **References**

512 Ainsworth, E. A., Yendrek, C. R., Sitch, S., Collins, W. J., and Emberson, L. D.: The
513 effects of tropospheric ozone on net primary productivity and implications for
514 climate change, *Annu. Rev. Plant Biol.*, 63, 637–661,
515 <https://doi.org/10.1146/annurevarplant-042110-103829>, 2012.

516 Ball, J. T., Woodrow, I. E., and Berry, J. A.: A model predicting stomatal conductance
517 and its contribution to the control of photosynthesis under different environmental
518 conditions, *Prog. Photosynthesis*, Springer, Dordrecht, 4, 221–224, 1987.

519 Bellucci, M., Locato, V., Sharkey, T. D., Gara D. and Loreto, F.: Isoprene emission by
520 plants in polluted environments, *J PLANT INTERACT.*, 18:1, 2266463,
521 <https://doi.org/10.1080/17429145.2023.2266463>, 2023

522 Calatayud, V., Cerveró, J., and Sanz, M. J.: Foliar, physiological and growth responses
523 of four maple species exposed to ozone, *Water Air Soil Pollut.*, 185, 239–254,
524 <https://doi.org/10.1007/s11270-007-9446-5>, 2007.

525 Chou, M.-D. and Suarez, M.J.: An Efficient Thermal Infrared Radiation
526 Parameterization for Use in General Circulation Models. Technical Report, 85p.
527 1994.

528 Dickinson, R. E.: Land surface processes and climate – Surface albedos and energy
529 balance, *Adv. Geophys.*, 25, 305–353, [https://doi.org/10.1016/S0065-](https://doi.org/10.1016/S0065-2687(08)60176-4)
530 [2687\(08\)60176-4](https://doi.org/10.1016/S0065-2687(08)60176-4), 1983.

531 Emmons, L. K., Walters, S., Hess, P. G., Lamarque, J.-F., Pfister, G. G., Fillmore, D.,
532 Granier, C., Guenther, A., Kinnison, D., Laepple, T., Orlando, J., Tie, X., Tyndall,
533 G., Wiedinmyer, C., Baughcum, S. L., and Kloster, S.: Description and evaluation
534 of the Model for Ozone and Related chemical Tracers, version 4 (MOZART-4),
535 *Geosci. Model Dev.*, 3, 43–67, <https://doi.org/10.5194/gmd-3-43-2010>, 2010.

536 Farquhar, G. D., Caemmerer, S. V., and Berry, J. A.: A biochemical model of
537 photosynthetic CO₂ assimilation in leaves of C₃ species, *Planta*, 149, 78–90,
538 <https://doi.org/10.1007/bf00386231>, 1980.

539 Felzer, B., Kicklighter, D., Melillo, J., Wang, C., Zhuang, Q., and Prinn, R.: Effects of
540 ozone on net primary production and carbon sequestration in the conterminous
541 United States using a biogeochemistry model, *Tellus B*, 56, 230–248,
542 <https://doi.org/10.1111/j.1600-0889.2004.00097.x>, 2004.

543 Feng, Z., Hu, E., Wang, X., Jiang, L., and Liu, X.: Ground-level O₃ pollution and its
544 impacts on food crops in China: A review, *Environ. Pollut.*, 199, 42–48,

545 <https://doi.org/10.1016/j.envpol.2015.01.016>, 2015.

546 Gong, C., Lei, Y., Ma, Y., Yue, X., and Liao, H.: Ozone– vegetation feedback through
547 dry deposition and isoprene emissions in a global chemistry–carbon–climate
548 model, *Atmos. Chem. Phys.*, 20, 3841–3857, [https://doi.org/10.5194/acp-203841-](https://doi.org/10.5194/acp-203841-2020)
549 2020, 2020.

550 Gong, C., Yue ,X., Liao, H., and Ma, Y.: A humidity-based exposure index representing
551 ozone damage effects on vegetation, *Environ. Res. Lett.*, 16, 044030,
552 <https://doi.org/10.1088/1748-9326/abecbb>, 2021.

553 Grell, G. A., McKeen, S., Michalakes, J., Bao, J.-W., Trainer, M., and Hsie, E.-Y.: Real-
554 time simultaneous prediction of air pollution and weather during the Houston 2000
555 Field Experiment, presented at the 4th Conference on Atmospheric Chemistry:
556 Atmospheric Chemistry and Texas Field Study, 13–17 January, American
557 Meteorological Society, Orlando, 2002.

558 Grell, G. A., Peckham, S. E., Schmitz, R., McKeen, S. A., Frost, G., Skamarock, W. C.,
559 and Eder, B.: Fully coupled “online” chem- istry within the WRF model. *Atmos.*
560 *Environ.*, 39, 6957–6975, <https://doi.org/10.1016/j.atmosenv.2005.04.027>, 2005.

561 Guenther, A., Karl, T., Harley, P., Wiedinmyer, C., Palmer, P. I., and Geron, C.:
562 Estimates of global terrestrial isoprene emissions using MEGAN (Model of
563 Emissions of Gases and Aerosols from Nature), *Atmos. Chem. Phys.*, 6, 3181–
564 3210, <https://doi.org/10.5194/acp-6-3181-2006>, 2006.

565 Hersbach, H., Bell, B., Berrisford, P., Hirahara, S., Horányi, A., Muñoz-Sabater, J.,
566 Nicolas, J., Peubey, C., Radu, R., Schepers, D., Simmons, A., Soci, C., Abdalla,
567 S., Abellan, X., Balsamo, G., Bechtold, P., Biavati, G., Bidlot, J., Bonavita, M., De
568 Chiara, G., Dahlgren, P., Dee, D., Diamantakis, M., Dragani, R., Flemming, J.,
569 Forbes, R., Fuentes, M., Geer, A., Haimberger, L., Healy, S., Hogan, R. J., Hólm,
570 E., Janisková, M., Keeley, S., Laloyaux, P., Lopez, P., Lupu, C., Radnoti, G., de
571 Rosnay, P., Rozum, I., Vamborg, F., Villaume, S., and Thépaut, J.-N.: The ERA5
572 global reanalysis, *Q. J. Roy. Meteor. Soc.*, 146, 1999–2049, 2020.

573 Hong, S.-Y., Noh, Y., and Dudhia, J.: A new vertical diffusion package with explicit

574 treatment of entrainment processes, *Mon. Weather Rev.*, 134, 2318–2341,
575 <https://doi.org/10.1175/MWR3199.1>, 2006.

576 Hu, J., Chen, J., Ying, Q., and Zhang, H.: One-year simulation of ozone and particulate
577 matter in China using WRF/CMAQ modeling system, *Atmos. Chem. Phys.*, 16,
578 10333–10350, <https://doi.org/10.5194/acp-16-10333-2016>, 2016.

579 Jin, Z., Yan, D., Zhang, Z., Li, M., Wang, T., Huang, X., Xie, M., Li S and Zhuang.:
580 Effects of elevated ozone exposure on regional meteorology and air quality in
581 China through ozone-vegetation coupling. *J. Geophys. Res.-Atmos.*, 128,
582 e2022JD038119. <https://doi.org/10.1029/2022JD038119>, 2023.

583 Li, J., Mahalov, A., and Hyde, P.: Simulating the impacts of chronic ozone exposure on
584 plant conductance and photosynthesis, and on the regional hydroclimate using
585 WRF/Chem, *Environ. Res. Lett.*, 11, 114017,
586 <https://doi.org/10.1088/17489326/11/11/114017>, 2016.

587 Li, P., Calatayud, V., Gao, F., Uddling, J., and Feng, Z. Z.: Differences in ozone
588 sensitivity among woody species are related to leaf morphology and antioxidant
589 levels, *Tree Physiol.*, 36, 1105– 1116, <https://doi.org/10.1093/treephys/tpw042>,
590 2016.

591 Li, P., Feng, Z., Catalayud, V., Yuan, X., Xu, Y., and Paoletti, E.: A meta-analysis on
592 growth, physiological, and biochemical responses of woody species to ground-
593 level ozone highlights the role of plant functional types, *Plant Cell Environ.*, 40,
594 2369–2380, <https://doi.org/10.1111/pce.13043>, 2017.

595 Liu, Y. and Wang, T.: Worsening urban ozone pollution in China from 2013 to 2017 –
596 Part 1: The complex and varying roles of meteorology, *Atmos. Chem. Phys.*, 20,
597 6305–6321, <https://doi.org/10.5194/acp-20-6305-2020>, 2020.

598 Lombardozzi, D., Levis, S., Bonan, G., and Sparks, J. P.: Predicting photosynthesis and
599 transpiration responses to ozone: decoupling modeled photosynthesis and stomatal
600 conductance, *Biogeosciences*, 9, 3113–3130, <https://doi.org/10.5194/bg-9-31132012>,
601 2012.

602 Lombardozzi, D., Sparks, J. P., and Bonan, G.: Integrating O₃ influences on terrestrial

603 processes: photosynthetic and stomatal response data available for regional and
604 global modeling, *Biogeosciences*, 10, 6815–6831, [https://doi:10.5194/bg-10-](https://doi:10.5194/bg-10-6815-2013)
605 6815-2013, 2013.

606 Lombardozzi, D., Levis, S., Bonan, G., Hess, P. G., and Sparks, J. P.: The influence of
607 chronic ozone exposure on global carbon and water cycles, *J. Climate*, 28, 292–
608 305, <https://doi.org/10.1175/JCLI-D-14-00223.1>, 2015.

609 Matyssek, R., Sandermann, H., Wieser, G., Booker, F., Cieslik, S., Musselman, R., and
610 Ernst, D.: The challenge of making ozone risk assessment for forest trees more
611 mechanistic, *Environ. Pollut.*, 156, 567–582,
612 <https://doi:10.1016/j.envpol.2008.04.017>, 2008.

613 Mlawer, E. J., Taubman, S. J., Brown, P. D., Iacono, M. J., and Clough, S. A.: Radiative
614 transfer for inhomogeneous atmosphere: RRTM, a validated correlated-k model
615 for the longwave, *J. Geophys. Res-Atmos.*, 102(D14), 16 663–16 682,
616 <https://doi.org/10.1029/97JD00237>, 1997.

617 Monks, P. S., Archibald, A. T., Colette, A., Cooper, O., Coyle, M., Derwent, R., Fowler,
618 D., Granier, C., Law, K. S., Mills, G. E., Stevenson, D. S., Tarasova, O., Thouret,
619 V., von Schneidmesser, E., Sommariva, R., Wild, O., and Williams, M. L.:
620 Tropospheric ozone and its precursors from the urban to the global scale from air
621 quality to short-lived climate forcer, *Atmos. Chem. Phys.*, 15, 8889–8973,
622 <https://doi.org/10.5194/acp-15-8889-2015>, 2015.

623 Morrison, H., Thompson, G., and Tatarskii, V.: Impact of cloud microphysics on the
624 development of trailing stratiform precipitation in a simulated squall line:
625 comparison of one- and two-moment schemes, *Monthly Weather Review*, 137,
626 991–1007, <https://doi.org/10.1175/2008MWR2556.1>, 2009.

627 Niu, G. Y., Yang, Z. L., Mitchell, K. E., Chen, F., Ek, M. B., Barlage, M., Kumar, A.,
628 Manning, K., Niyogi, D., Rosero, E., Tewari, M., and Xia, Y.: The community
629 Noah land surface model with multiparameterization options (Noah-MP): 1.
630 Model description and evaluation with local-scale measurements, *J. Geophys.*
631 *Res-Atmos.*, 116, D12, <https://doi.org/10.1029/2010JD015139>, 2011.

632 Ren, W., Tian, H., Tao, B., Chappelka, A., Sun, G., Lu, C., Liu, M., Chen, G., and Xu,
633 X.: Impacts of tropospheric ozone and climate change on net primary productivity
634 and net carbon exchange of China's forest ecosystems, *Glob. Ecol. Biogeogr.*, 20,
635 391–406, <https://doi.org/10.1111/j.1466-8238.2010.00606.x>, 2011.

636 Sadiq, M., Tai, A. P. K., Lombardozzi, D., and Val Martin, M.: Effects of ozone–
637 vegetation coupling on surface ozone air quality via biogeochemical and
638 meteorological feedbacks, *Atmos. Chem. Phys.*, 17, 3055–3066,
639 <https://doi.org/10.5194/acp-17-3055-2017>, 2017.

640 Sitch, S., Cox, P. M., Collins, W. J., and Huntingford, C.: Indirect radiative forcing of
641 climate change through ozone effects on the land-carbon sink, *Nature*, 448, 791–
642 794, <https://doi.org/10.1038/nature06059>, 2007.

643 Skamarock W C and Klemp J B. A time-split nonhydrostatic atmospheric model for
644 weather research and forecasting applications. *J. Comput. Phys.*, 227(7): 3465-
645 3485, <https://doi.org/10.1016/j.jcp.2007.01.037>, 2008.

646 Su, B., Zhou, M., Xu, H., Zhang, X., Li, Y., Su, H., and Xiang B.: Photosynthesis and
647 biochemical responses to elevated O₃ in *Plantago major* and *Sonchus oleraceus*
648 growing in a lowland habitat of northern China, *J. Environ. SCI.*, 53(3): 113-121,
649 <https://doi.org/10.1016/j.jes.2016.05.011>, 2017.

650 Tie, X. X., Madronich, S., Walters, S., Zhang, R. Y., Rasch, P., and Collins, W.: Effect
651 of clouds on photolysis and oxidants in the troposphere, *J. Geophys. Res.-Atmos.*,
652 108, 4642, <https://doi.org/10.1029/2003jd003659>, 2003.

653 Wan, W., Manning, WJ., Wang, X., Zhang, H., Sun, X., and Zhang, Q.: Ozone and
654 ozone injury on plants in and around Beijing, China, *Environ Pollut.*, 191: 215-
655 222, <https://doi.org/10.1016/j.envpol.2014.02.035>, 2014

656 Wilkinson, S., Clephan, A. L., and Davies, W. J.: Rapid Low Temperature-Induced
657 Stomatal Closure Occurs in Cold-Tolerant *Commelina Communis* Leaves But Not
658 in Cold-Sensitive Tobacco Leaves, via a Mechanism That Involves Apoplastic
659 Calcium But Not Abscisic Acid. *Plant Physiol.*, 126, 1566–1578.
660 <https://doi.org/10.1104/pp.126.4.1566>, 2001.

661 Wittig, V. E., Ainsworth, E. A., and Long, S. P.: To what extent do current and projected
662 increases in surface ozone affect photosynthesis and stomatal conductance of trees?
663 A metaanalytic review of the last 3 decades of experiments, *Plant Cell Environ.*,
664 30, 1150–1162, <https://doi.org/10.1111/j.13653040.2007.01717.x>, 2007.

665 Xie, X., Wang, T., Yue, X., Li, S., Zhuang, B., Wang, M., and Yang, X.: Numerical
666 modeling of ozone damage to plants and its effects on atmospheric CO₂ in China,
667 *Atmos. Environ.*, 217, 116970, <https://doi.org/10.1016/j.atmosenv.2019.116970>,
668 2019.

669 Yue, X. and Unger, N.: Ozone vegetation damage effects on gross primary productivity
670 in the United States, *Atmos. Chem. Phys.*, 14, 9137–9153,
671 <https://doi.org/10.5194/acp-14-9137-2014>, 2014.

672 Yue, X. and Unger, N.: The Yale Interactive terrestrial Biosphere model version 1.0:
673 description, evaluation and implementation into NASA GISS ModelE2, *Geosci.*
674 *Model Dev.*, 8, 2399–2417, <https://doi.org/10.5194/gmd-8-2399-2015>, 2015.

675 Zaveri, R. A., and Peters, L. K.: A new lumped structure photochemical mechanism for
676 large-scale applications, *J Geophys Res-Atmos*, 104, 30387-30415, 1999.

677 Zaveri, R. A., Easter, R. C., Fast, J. D., and Peters, L. K.: Model for simulating aerosol
678 interactions and chemistry (MOSAIC), *J. Geophys. Res-Atmos.*, 113, D13204,
679 <https://doi.org/10.1029/2007JD008782>, 2008.

680 Zhou, S. S., Tai, A. P. K., Sun, S., Sadiq, M., Heald, C. L., and Geddes, J. A.: Coupling
681 between surface ozone and leaf area index in a chemical transport model: strength
682 of feedback and implications for ozone air quality and vegetation health, *Atmos.*
683 *Chem. Phys.*, 18, 14133–14148, <https://doi.org/10.5194/acp-18-14133-2018>, 2018.

684 Zhu, J., Tai, A. P. K., and Yim, S. H. L.: Effects of ozone-vegetation interactions on
685 meteorology and air quality in China using a two-way coupled land-atmosphere
686 model, *Atmos. Chem. Phys.*, 22, 765-782, [https://doi.org/10.5194/acp-22-765-](https://doi.org/10.5194/acp-22-765-2022)
687 2022, 2022.

688

689 **Tables**690 **Table 1.** Parameters used for S2007 O₃ damage scheme.

PFTs ^a	$a_{PFT}(\text{nmol}^{-1} \text{m}^2 \text{s})$ ^b	$\gamma_{PFT}(\text{nmol m}^{-2} \text{s}^{-1})$
EBF	0.075, 0.02	1.6
NF	0.075, 0.02	1.6
DBF	0.15, 0.04	1.6
SHR	0.1, 0.03	1.6
GRA	1.4, 0.25	5
CRO	1.4, 0.25	5

691 ^a The plant functional types (PFTs) include evergreen broadleaf forest (EBF), needleleaf
692 forest (NF), deciduous broadleaf forest (DBF), shrubland (SHR), grassland (GRA), and
693 cropland (CRO).

694 ^b The first number is for high sensitivity and the second is for low sensitivity.

695

696

697

Table 2. Slopes and intercepts used for L2013 O₃ damage scheme.

PFTs	a_p (mmol m ⁻²)	b_p	a_c (mmol m ⁻²)	b_c
EBF	0	0.8752	0	0.9125
NF	0	0.839	0.0048	0.7823
DBF	0	0.8752	0	0.9125
SHR	0	0.8752	0	0.9125
GRA	-0.0009	0.8021	0	0.7511
CRO	-0.0009	0.8021	0	0.7511

698

699

700

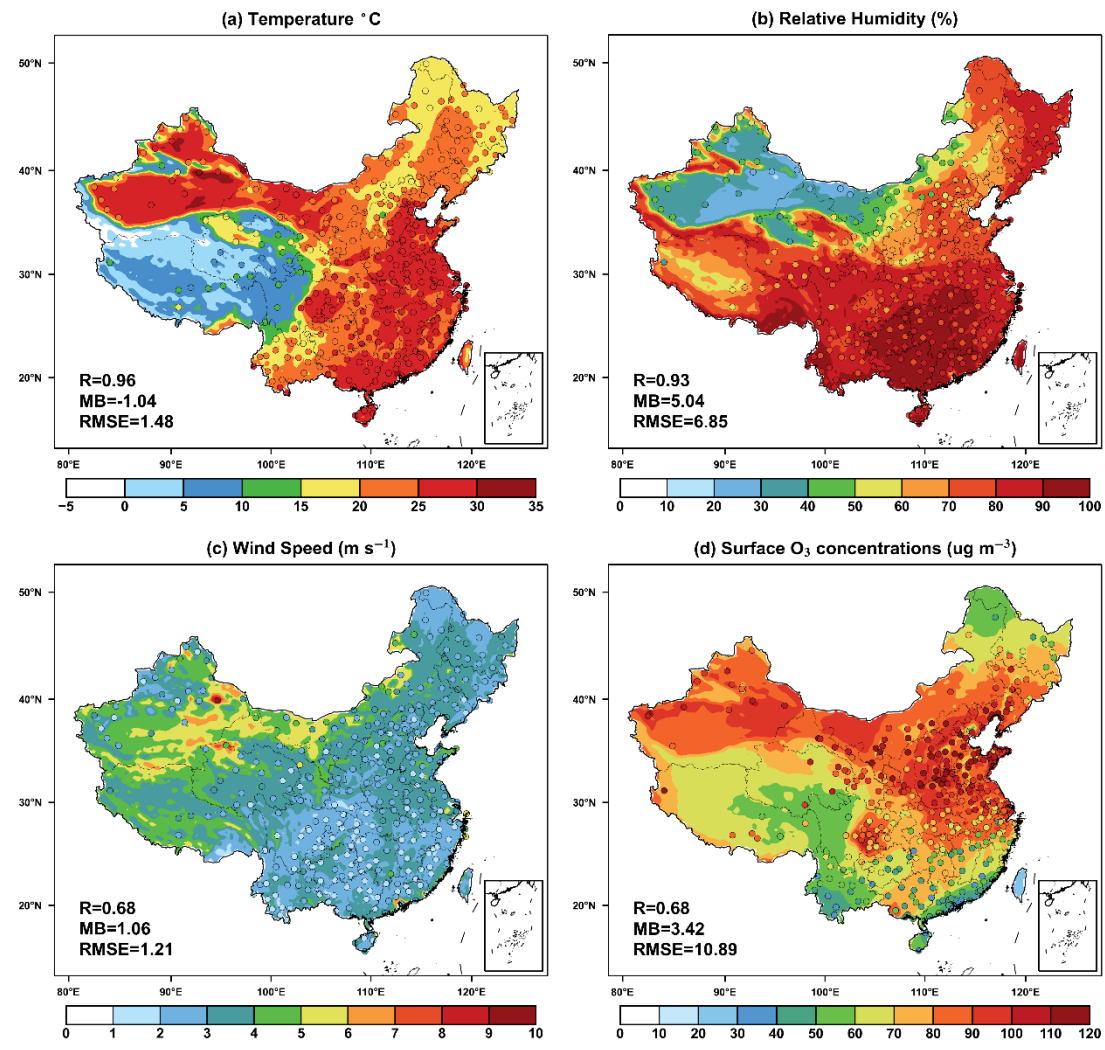
701

Table 3. Summary of simulation experiments

Name	O ₃ damage to vegetable	Scheme
CRTL	-	-
Offline_SH07	High	Sitch et al. (2007)
Offline_SL07	Low	Sitch et al. (2007)
Offline_L13	-	Lombardozzi et al. (2013)
Online_SH07	High	Sitch et al. (2007)
Online_SL07	Low	Sitch et al. (2007)
Online_L13	-	Lombardozzi et al. (2013)

702

703



705

706

707

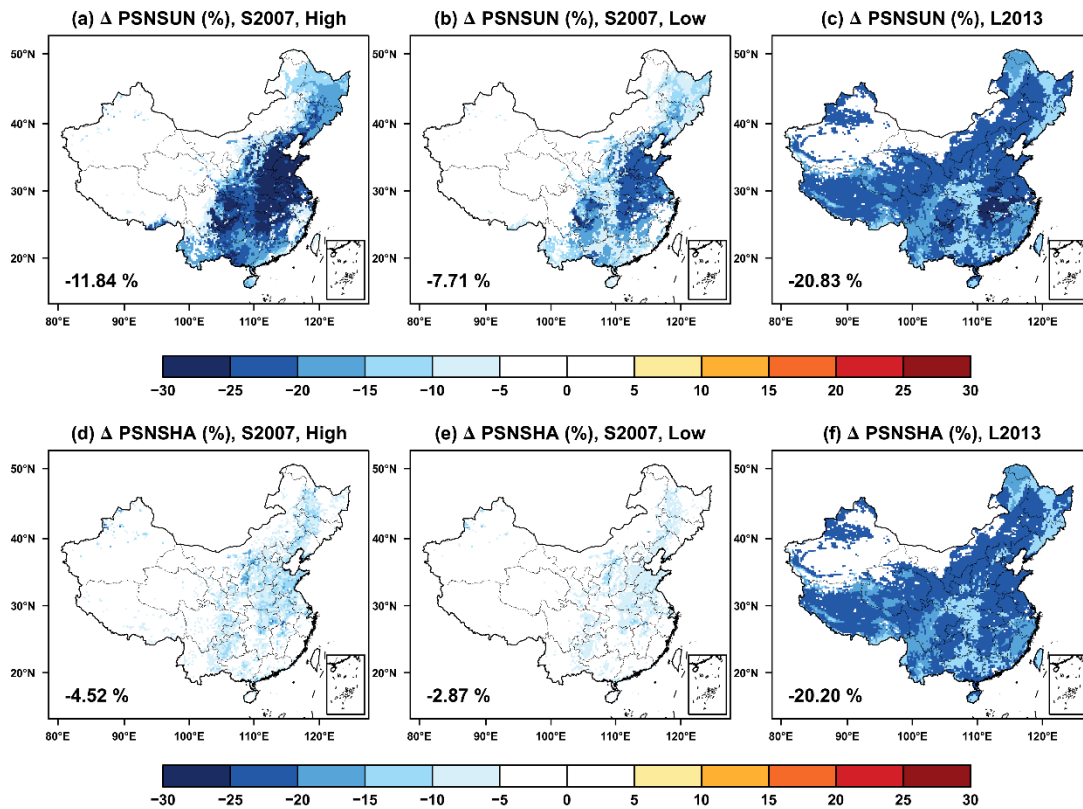
708 **Figure 1** Evaluations of simulated summer (June–August) daily (24-h average) (a)709 near-surface temperature, (b) relative humidity, (c) wind speed, and (d) surface O_3

710 concentrations in China. The dots represent the site-level observations. The correlation

711 coefficients (R), mean biases (MB), and root-mean-square error (RMSE) for the

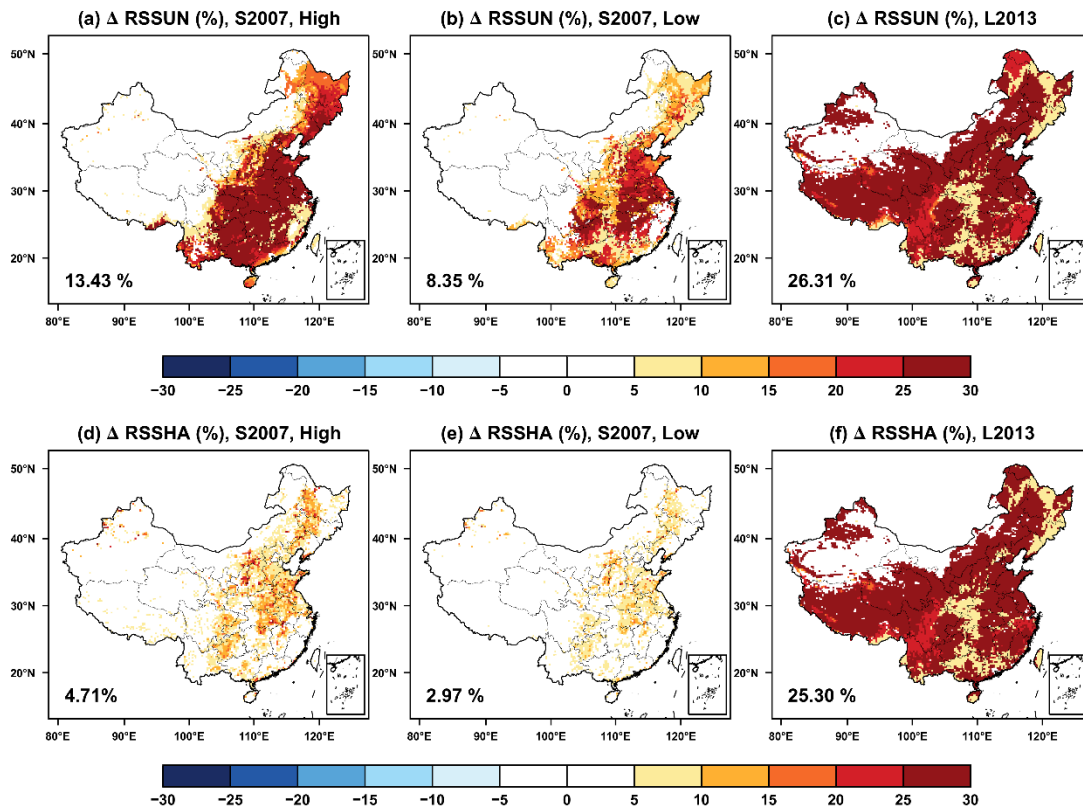
712 comparisons are shown in the lower left corner of each panel.

713



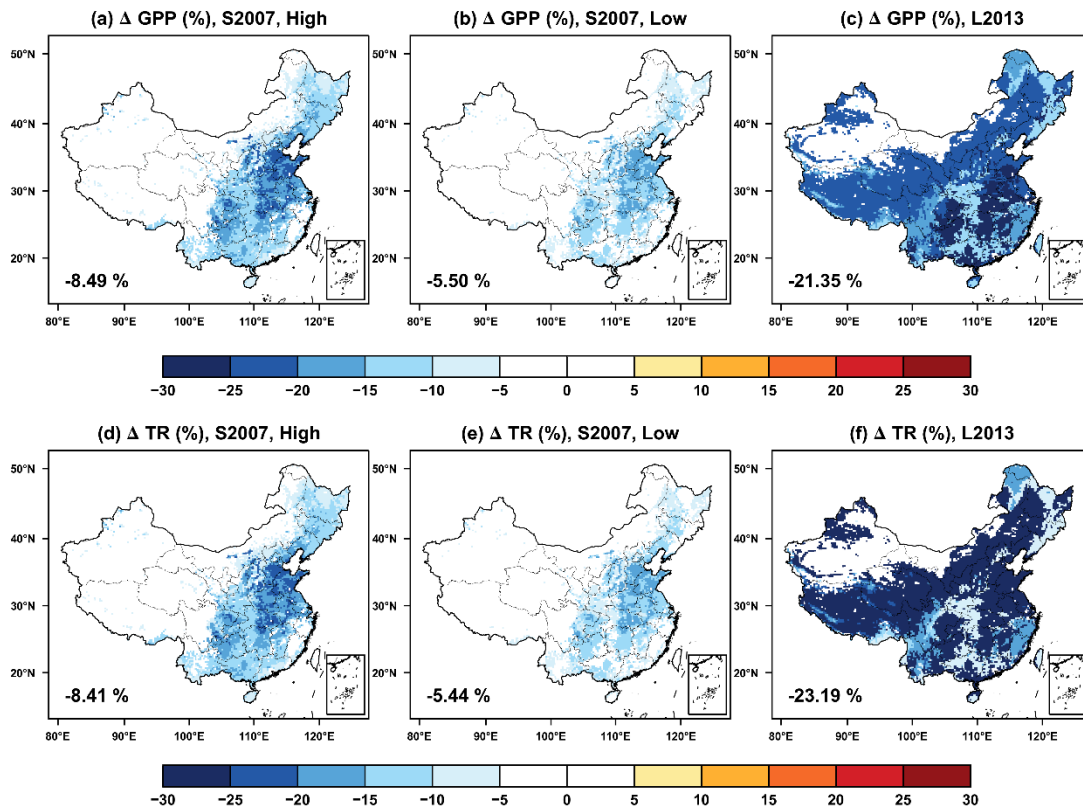
714
 715
 716
 717
 718
 719
 720

Figure 2 Offline O₃ damage (%) to the summertime photosynthesis of (a-c) sunlit and (d-f) shaded leaves predicted by the S2007 scheme with (a, d) high and (b, e) low sensitivities or the (c, f) L2013 scheme. The area-weighted percentage changes are shown in the lower left corner.



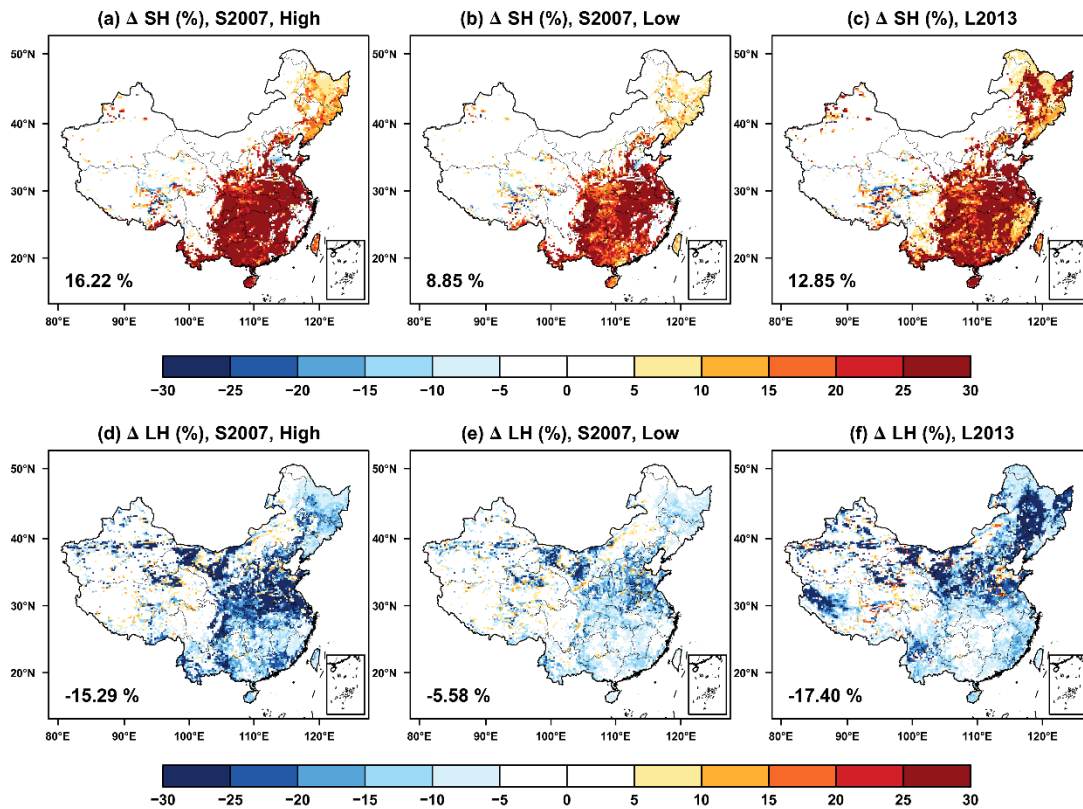
721
722
723
724

Figure 3 The same as Figure 2 but for the changes in stomatal resistance.



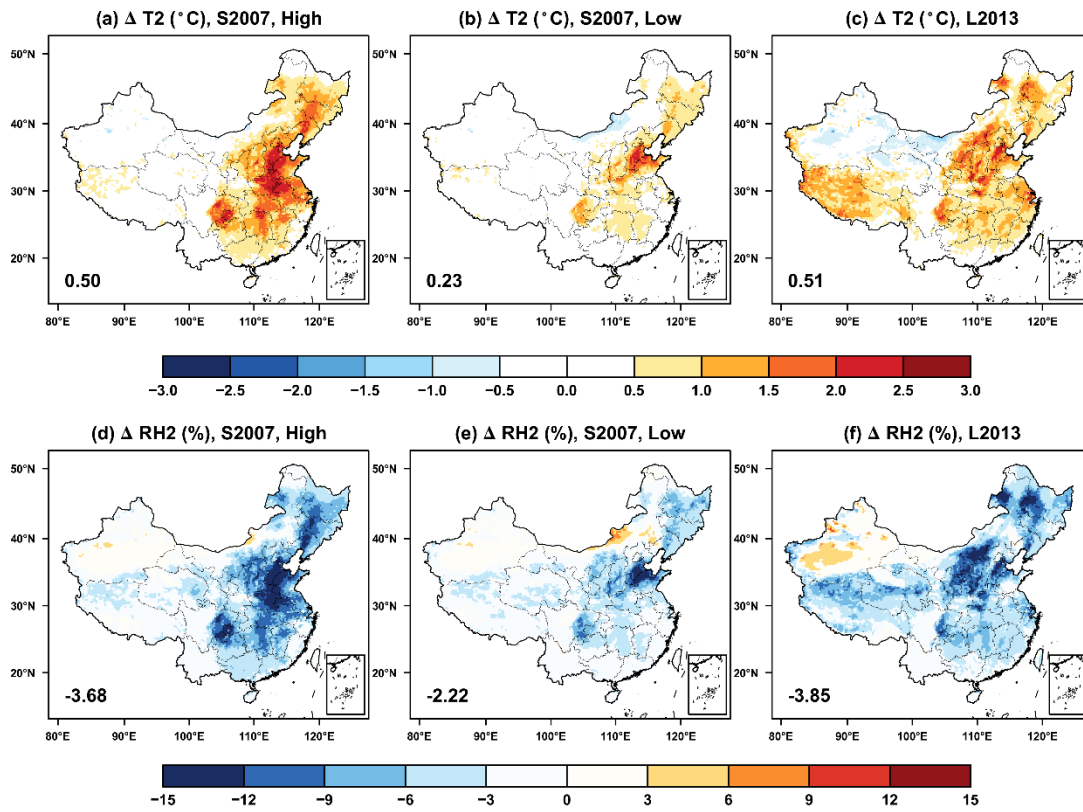
725
726
727
728
729
730
731

Figure 4 Offline O₃ damage (%) to the (a-c) gross primary productivity (GPP) and (d-f) transpiration rate (TR) predicted by the Sitch scheme with (a, d) high and (b,e) low sensitivities or the (c, f) Lombardozzi scheme. The area-weighted percentage changes are shown in the lower left corner.



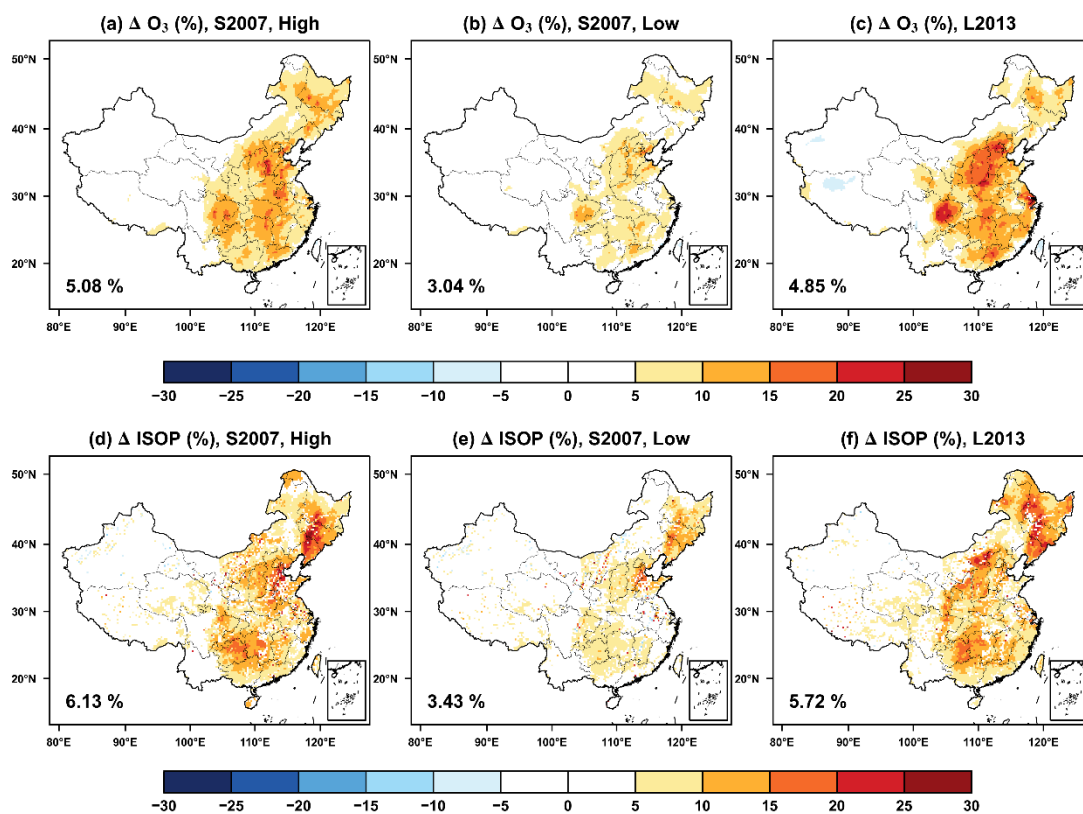
732
 733
 734
 735
 736
 737
 738
 739

Figure 5 The feedback of O₃-vegetation interaction to surface (a-c) sensible and (d-f) latent heat fluxes in the summer predicted by the S2007 scheme with (a, d) high and (b, e) low sensitivities or the (c, f) L2013 scheme. The relative changes are shown with area-weighted percentage changes indicated at the lower left corner.



740
 741
 742
 743
 744
 745

Figure 6 The same as Figure 5 but for changes in (top) air temperature and (bottom) relative humidity at 2 meters.



747

748

749 **Figure 7** The feedback of O₃-vegetation interaction to surface O₃ concentrations and
 750 isoprene emissions in the summer predicted by the S2007 scheme with (a, d) high and
 751 (b, e) low sensitivities or the (c, f) L2013 scheme. The area-weighted percentage
 752 changes are shown in the lower left corner.

753